Journal of Hazardous Materials 425 (2022) 127818

Contents lists available at ScienceDirect

Journal of Hazardous Materials

journal homepage: www.elsevier.com/locate/jhazmat

Metabolomic and transcriptomic investigation of the mechanism involved in enantioselective toxicity of imazamox in *Lemna minor*

Rui Li, Chenxi Luo, Jingsi Qiu, Yuanfu Li, Hui Zhang, Huihua Tan *

Guangxi key laboratory of Agric-Environment and Agric-products Safety, National Demonstration Center for Experimental Plant Science Education, College of Agriculture, Guangxi University, Nanning, Guangxi 530004, People's Republic of China

ARTICLE INFO

Keywords:
Imazamox
Enantioselective toxicity mechanisms
Multi-omics
Lemna minor

ABSTRACT

Imazamox (IM) is a chiral pesticide that has been widely used in agriculture. Currently, few studies have investigated the toxicity mechanisms of imazamox to aquatic macrophyte from the enantiomer level. In this study, the enantioselective effects of IM on the toxicity and physiological and biochemical system of aquatic macrophyte *Lemna minor* were systematically investigated. Metabolomic and transcriptomic for *Lemna minor* were used to identify potential mechanisms of toxicity. 7 d EC_{50}s for racemic-, *R*-, and *S*-IM were 0.036, 0.035, and 0.203 mg/L, respectively, showing enantioselective toxicity. In addition, IM caused *Lemna minor* lipid peroxidation and antioxidant damage, and inhibited the activities of the target enzymes. Metabolomic and transcriptomic data indicated that *R*-IM interferenced differentially expressed genes and metabolites of *Lemna minor* which were enriched in carbon fixation during photosynthesis, glutathione metabolic pathway, pentose phosphate pathway, zeatin biosynthesis, and porphyrin and chlorophyll metabolism. *S*-IM affected phenylalanine metabolism, phenylpropanoid biosynthesis, zeatin biosynthesis and secondary metabolite biosynthesis. Racemic-IM influenced carbon fixation during operation, glutathione metabolic pathway, zeatin biosynthesis and pentose phosphate pathway. The results provide new insights into the enantioselective toxicity mechanisms of IM to *Lemna minor*, and lay the foundation for conducting environmental risk assessments.

1. Introduction

The amount of pesticides used around the world has increased exponentially over the past few decades. As of the year 2017, about 4.1 million tonnes of pesticides were used globally (FAOSTAT, 2017). However, less than 1% of the amount of pesticide applied actually reaches the target organisms, and most of the remainder is deposited directly onto the soil (Chiaia-Hernandez et al., 2017). The resulting high pesticide residue concentrations in soil then pollute the aquatic environment through runoff or leaching from the soil. The presence of the aquatic macrophyte *Lemna minor* (*L. minor*) has major effects on the structure, function, and stability of aquatic ecosystems (Park et al., 2012). Because *L. minor* are small in size, grow quickly, and are sensitive to pollutants, it is considered to be an ideal test species for determining the phytotoxicities and environmental risks posed by pesticides (Lewis et al., 1995). In previous studies, tests using *L. minor* have been used to investigate the toxic effects of pesticides such as atrazine, flurochloridone, and lactofen and their metabolites in the aquatic environment (Klementová et al., 2019; Wang et al., 2016a; Zhou et al., 2020). However, few in-depth studies of the toxicities of pesticides to *L. minor* have been performed.

Imazamox (IM) (Fig. 1) is a chiral imidazolinone pesticide that is widely applied to peanut and soybean fields. IM inhibits synthesis of branched amino acids by inhibiting acetolactate synthetase. The different enantiomers of chiral pesticides have different biological activities, toxicities, and environmental behaviors (Asada et al., 2017).

Abbreviations: MDA, Malondialdehyde; SOD, Superoxide dismutase; CAT, Catalase; POD, Peroxidase; GSH, Glutathione; ALS, Acetolactate synthase; ATP, Adenosine triphosphate; GluTR, glutamyl-tRNA; Glu, Glutamic acid; GSA, glutamate-1-semialdehyde; GSSG, Glutathiol; RuBP, Ribulose-1,5-bisphosphate; RBCS, ribulose-bisphosphate carboxylase small chain; 3PG, 3-phosphoglycerate; PK, phosphoglycerate kinase; 1, 3-BPG, 1, 3-bisphosphoglycerate; G3P, glyceraldehyde 3-phosphate; GAPD, Glyceraldehyde-3-phosphate dehydrogenase; R5P, Ribulose 5-phosphate; Ru5P, ribulose 5-phosphate; G6P, glucose 6-phosphate; 6PGDH, 6-phosphogluconate dehydrogenase enzymes; 6PGA, 6-Phosphogluconic Acid; NADPH, nicotinamide adenine dinucleotide phosphate; AMP, Adenosine monophosphate; ADP, adenosine diphosphate; PAL, phenylalanine ammonialyase; C4H, Cinnamate 4-hydroxylase; CCoAOMT, caffeoyl-CoA O-methyltransferase.

* Corresponding author.
E-mail address: tanhh@gxu.edu.cn (H. Tan).

https://doi.org/10.1016/j.jhazmat.2021.127818
Received 16 September 2021; Received in revised form 3 November 2021; Accepted 14 November 2021
Available online 22 November 2021

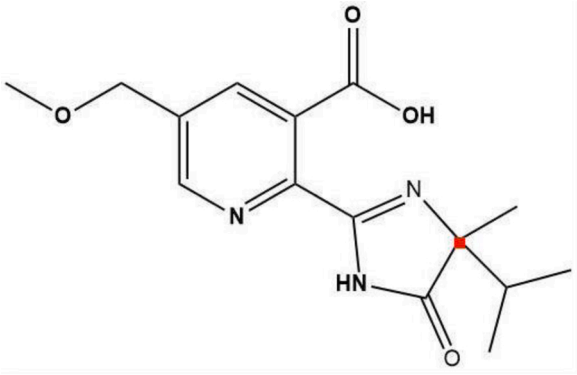

Fig. 1. Structure of imazamox.

Increasing attention is being paid to the enantioselective effects of chiral pesticides (Ye et al., 2015). IM has been found to be enantioselectively toxic to maize roots (Wei et al., 2016). Enantioselective degradation and bioaccumulation of IM have been studied in earthworm–soil microcosms (Hu et al., 2020). IM only weakly adsorbs to soil, and so is mobile in soil (Cessna et al., 2012). Because of this mobility, IM can be transferred to the aquatic environment in surface runoff and through leaching, and can pose serious risks to aquatic ecosystems (Sikorski et al., 2019). However, the enantioselective toxicity of IM to aquatic macrophyte and the mechanisms involved have not been reported.

Omics techniques can provide accurate information on molecular disturbances in certain cells and tissues induced by the presence of certain substances (Purkait et al., 2021). Because biological systems are dynamic and heterogeneous, it is very hard to decipher all the mechanism involved. However, multi-omics association analyses can adequately elucidate the response pathways of organisms exposed to chemical substances and thus identify mechanisms that may be involved in toxicity. Therefore, multi-omics techniques have been widely used to explore the toxic mechanisms of pollutants. For example, Yang integrated multi-omics to investigate the mechanism of intestinal toxicity in earthworms exposed to TNBP (Yang et al., 2020). Tian explored the impact of bisphenol A and tetrabromobisphenol A on the endocannabinoid system of zebrafish by metabolomics and transcriptomics (Tian et al., 2021). Lee used multi-omics to reveal the underlying molecular mechanisms of the developmental neurotoxicity of perfluorooctanesulfonic acid to zebrafish (Lee et al., 2021).

This study aimed to comprehensively and systematically investigate the mechanisms involved in the enantioselective toxicity of IM to *L. minor* in terms of growth, physiology and biochemistry, and thus improve environmental risk evaluations and pesticide application management programs. To our knowledge, this was the first study to use the powerful and promising metabolomic and transcriptomic methods to analyze the enantioselective toxicity mechanisms of IM to *L. minor*.

2. Materials and methods

2.1. Chemicals and reagents

A racemic (Rac) IM (>98.0% pure; Dr. Ehrenstorfer) analytical standard was purchased from LGC (Teddington, UK). Chiral separations were performed using an Agilent 1290 Infinity II HPLC system (Agilent Technologies, Santa Clara, CA, USA). The instrument conditions and the method used to determine the absolute configurations of the enantiomers were described in a previous publication (Li et al., 2019a).

All of the other chemicals used in the study were purchased from the Tianjin Damao Chemical Reagent Factory (Tianjin, China). Water was purified using a Milli-Q system (Merck, Darmstadt, Germany). Working racemic and enantiomers IM solutions were prepared by diluting the stock (1000 mg/L) solution with ultra-pure water and then stored at 4 °C.

2.2. Plant material and cultivation

The *L. minor* culture used in the study was provided by Yike Shifu Technology Co. (Beijing, China). The *L. minor* was first washed with 0.01 M NaClO for 1 min to disinfect the surfaces, then the *L. minor* was washed three times with sterile water. Genetic consistency was ensured by selecting healthy *L. minor* plants and then culturing these parent plants under laboratory conditions for three weeks before use in this study. The *L. minor* plants were cultured in sterile Steinberg nutrient solution with a stable pH between 5.3 and 5.7. The incubation and test conditions were: 24 ± 2 °C, 16 h light/8 h dark photoperiod, 55% relative air humidity, and 144 μmol/(m^2 s) irradiance (provided by a plant growth lamp).

2.3. Growth inhibition tests

Growth inhibition tests were performed following the Chinese agricultural industry standard NY/T 3090–2007. All glassware was chemically disinfected and cleaned before use. A 100 mL aliquot of Steinberg nutrient solution containing a specified concentration of IM was added to a 500 mL beaker. Then six healthy *L. minor* plants each with three leaves were placed in the beaker. Tests were performed at Rac-IM concentrations between 0.018 and 0.091 mg/L, *R*-IM concentrations between 0.023 and 0.066 mg/L, and *S*-IM concentrations between 0.100 and 0.623 mg/L. The experiment was conducted in triplicates. In addition, three controls in the presence of equal amount of ultra-pure water were performed. Each test was performed for 7 d, and the number of leaves on each plant was recorded once each day.

2.4. Calculating EC_{50} values

Mean biomass inhibition, as a percentage, was calculated as described in the Chinese agricultural industry standard NY/T3090–2007, using the equation1 (eq 1).

$$I = ((bc - bt)/bc) \times 100 \quad (1)$$

Where I is mean biomass inhibition as a percentage, bc is the difference between the final amount of biomass and the initial amount of biomass for the control group, and bt is the difference between the final amount of biomass and the initial amount of biomass for the treatment group. The EC_{50} was determined from the curve found by plotting the logarithms of the inhibition values against the logarithms of the IM concentrations.

2.5. Determining photosynthetic pigments

A 0.2-g aliquot of *L. minor* leaves was ground in a mortar with cold 80% acetone in water. The mixture was then centrifuged at 10,000 × *g* for 10 min. The photosynthetic pigment concentrations in the supernatant were then determined. The absorbance values at 470, 647, and 663 nm were used to calculate the chlorophyll *a*, chlorophyll *b*, and carotenoid concentrations using the eqs 2–5 (Lichtenthaler, 1987).

$$[Chlorophylla] = 12.25A_{663} - 2.79A_{647} \quad (2)$$

$$[Chlorophyllb] = 21.50A_{647} - 5.10A_{663} \quad (3)$$

$$[Totalchlorophyll] = 7.15A_{663} + 18.71A_{647} \quad (4)$$

$$[Carotenoids] = (1000A_{470} - 1.82[Chlorophylla] - 85.02[Chlorophyllb])/198 \quad (5)$$

Where A_{470}, A_{647}, and A_{663} are the absorbance values at 470, 647, and 663 nm, respectively.

2.6. Determining proteins, antioxidant enzyme activities, and lipid peroxidation

A 0.2-g aliquot of *L. minor* leaves were ground in a mortar with phosphate-buffered saline at pH 7.4 in an ice bath. Three replicate samples treated at each test concentration were extracted. The mixture was centrifuged at 1000 × *g* for 10 min, then the antioxidant enzyme activities, malondialdehyde (MDA) content, and soluble protein content of the supernatant were determined. The catalase (CAT), glutathione, peroxidase (POD), and superoxide dismutase (SOD) activities and the MDA and soluble protein contents were determined using commercial kits (Jiancheng Bioengineering Institute, Nanjing, China).

2.7. Determining the target enzyme acetolactate synthetase

The presence of IM inhibits acetolactic synthase (ALS) production and decreases the amounts of isoleucine, leucine, and valine that are synthesized, impedes DNA synthesis and cell division, and then prevents the synthesis of some functional proteins, meaning a plant exposed to IM will die (Qian et al., 2013). Therefore, the ALS activity was measured to explore the effect of IM on the activity of this target enzyme in *L. minor*. A double antibody one-step sandwich enzyme-linked immunosorbent assay was used to determine acetolactate synthase (ALS). Samples, standard substances, and detection antibodies labeled with horseradish peroxidase were successively added to microporous systems coated with ALS antibodies, and then the microporous systems were incubated and thoroughly washed. The 3,3′,5,5′-tetramethylbenzidine substrate was turned blue by peroxidase and then yellow by acid. Absorbance at 450 nm was measured using a microplate reader. ALS activity was calculated using a calibration curve prepared by analyzing standards.

2.8. Metabolomic analysis by ultra-high-performance liquid chromatography electrospray ionization tandem mass spectrometry

Samples of *L. minor* from acute toxicity tests were vacuum freeze-dried and then ground using a mill at 30 Hz for 1.5 min 100 mg of a *L. minor* sample was weighed and extracted overnight at 4°C with 1 mL of a 70% aqueous methanol solution containing 0.1 mg/L lidocaine as an internal standard. The mixture was vortexed three times during the storage period to ensure that adequate extraction occurred. The mixture was centrifuged at 10,000 × *g* for 10 min and then the supernatant was passed through a membrane filter with 0.22 μm pores. The extract was then analyzed by liquid chromatography mass spectrometry. A 5 μL sample extract was used to prepare quality control samples. A quality control sample was analyzed after every 10 samples to assess the repeatability of the method. Metabolites in each sample were analyzed using an LC-ESI-MS/MS system (UPLC, Shim-pack UFLC SHIMADZU CBM20A, MS/MS (Applied Biosystems 4500 QTRAP). The conditions that were used were described in a previous publication (Wang et al., 2018). The data were processed using Analyst 1.6.1 software (AB SCIEX, Framingham, MA, USA). The data filtering, peak detection, comparison, calculation, and metabolite identification methods that were used were described in a previous publication (Tang et al., 2019). Metabolites were found to be different if a T-test P value was < 0.05 and the variable importance plot value was ≥ 1. The data were mapped to a Kyoto Encyclopedia of Genes and Genomes (KEGG) metabolic pathway to allow pathway enrichment analysis to be performed (false discovery rate ≤ 0.05) (Kanehisa et al., 2008).

2.9. Transcriptome analysis

Total RNA was extracted from *L. minor* exposed to Rac-, *R*-, and *S*-IM each at a concentration of 0.036 mg/kg using Trizol kits (Invitrogen, China) following the instructions provided by the manufacturer. Each test was performed in triplicate. The total RNA that was extracted was treated with RNase-free DNase I (Takara, Dalian, China) at 25 °C for 15 min to remove residual DNA. The total RNA quantity and completeness were evaluated using a Bioanalyzer 2100 system (Agilent Technologies) and a Nano Drop ultraviolet spectrophotometer (Thermo Fisher Scientific). A NEBNext Ultra RNA library preparation kit (Gene, Beijing, China) was used to construct a cDNA library, and sequencing was performed using an Illumina HiSeq TM 2500 instrument (Genedenovo Biotechnology, Guangzhou, China). The content containing the adapter was read, and reads containing $> 10\%$ unknown nucleotides (N) and low-quality readings containing $> 50\%$ low-quality ($Q \leq 10$) bases were deleted to leave high-quality clean readings to facilitate the subsequent experiments. Bowtie2, a short reads alignment tool, was used to map the high-quality data with rRNA removed to the reference transcriptome, then the mapping ratio was calculated. RSEM software was used to quantify the gene abundances, and kilobases of transcripts per million mapped reads were used to quantify expression of individual genes (Li et al., 2011). The edgeR software package (http://www.rproject.org/) was then used to identify differentially expressed genes (DEGs), and a DEG was identified when $|\log_2 FC| \geq 1$ and false discovery rate < 0.05. The GOseq R software package (Young et al., 2010) and KOBAS software (Mao et al., 2005) were used to perform enrichment analysis of the gene ontology functions and KEGG pathways for the DEGs.

Quantitative real-time polymerase chain reaction (qRT-PCR) analyses were performed to verify the RNA sequencing data. *L. minor* samples were exposed to 0.036 mg/L of IM for each analysis. Three replicate samples in each treatment group were analyzed. The method that was used was described previously (Li et al., 2020). The primers used in the qRT-PCR analyses were shown in Table 1. And genes verified by qRT-PCR were randomly selected. The Actin gene was used as an internal reference gene.

2.10. Statistics

The data were statistically analyzed using SPSS 26.0 software (IBM, Armonk, NY, USA). Each test was performed at least three times. The significance of the differences of the average values between the treatments was evaluated by the one way analysis of variance (ANOVA, $p < 0.05$). The comparison of means was based on the method of Tukey's range test.

3. Results and discussion

3.1. Growth inhibition

The growth status of plants under stress resulting from the presence of pesticides has been assessed in many previous studies using the fresh weights of the plants. EC_{50} was often used as an important indicator to evaluate the acute toxicity of pollutants, the lower the EC_{50} was, the stronger the acute toxicity had (Chen et al., 2016; Zhang et al., 2016). In this study, acute toxicity data were calculated using the fresh weights of the *L. minor* plants. As shown in Table 2, the EC_{50}s for *L. minor* were about six times higher for Rac- and *R*-IM than for *S*-IM ($p < 0.05$) which

Table 1
Differentially expressed gene primers used for the quantitative real-time polymerase chain reaction analyses.

DEPs	Primer sequence	
	Forward sequence (5′−3′)	Reverse sequence (5′−3′)
Unigene0050294	GAGGTGGAGGCCCAAAAGTT	CGAGGCGAGCCTCATAAACA
Unigene0013690	TTGACCGATGGAGCAAGTCC	TTGAACCGTACGAGAGTGCC
Unigene0051266	CATGCATGCGCTCATAACCC	CCATCGGCAACAAATAGGCG
Unigene0049750	CCTGGATGACGTTTTGCTGC	AAGCCGTTAACACCCTCTCC
Unigene0050283	GAGTTTCAGACTCCGCCCAA	CCCTCCCCACATGCCATATC
Unigene0046680	TTGAACCCGCCTCTGGAATC	ACTGTCTTTGGTGAAGGCGT
Unigene0043337	CAGCAATTTCTGGGGCTTCG	TGAAGTAGCTCCGTCGGGTA
Actin3	AAGCTCGCTTATGTGGCACT	CCGCCCCGATAGTAATCACC

Table 2
EC_{50}s for racemic (Rac-) imazamox and the imazamox enantiomers to *Lemna minor* (on a fresh weight basis).

Pesticide	Regression equation	EC_{50} (mg L^{-1})	R^2
Rac-imazamox	Y= 10.110 + 7.026X	0.036	0. 956
R-imazamox	Y= 13.375 + 9.217X	0.035	0.956
S-imazamox	Y= 4.879 + 7.041X	0.203	0.985

indicated that the *R*- and *S*-IM enantiomers had enantioselective toxicities to *L. minor* . The enantioselective toxicities of imidazolinone herbicides to non-target organisms such as *Arabidopsis* and rice have been studied previously. In those studies, *R*-imidazolinones were found to be more toxic than *S*-imidazolinones (Qian et al., 2011; Wei et al., 2016).

The numbers of leaves on *L. minor* plants exposed to IM at different concentrations were recorded. The results are shown in Fig. 2. The number of leaves increased less as the IM concentration increased, as was also found in a previous study (Wang et al., 2016a). The number of *L. minor* leaves stopped increasing at a high IM concentration. This may have been because plants under environmental stress may stop growing and prepare for self-defense or dormancy (Tang et al., 2015).

According to the results of growth inhibition test, three different inhibitory concentrations (0.02, 0.08 and 0.5 mg/kg) were selected to explore the effects of IM on photosynthetic pigment, antioxidant system and target enzyme activity of *L. minor* from the enantiomer level.

3.2. Photosynthetic pigment content

Chlorophyll is an essential part of the photosynthesis process. Changes in the chlorophyll contents of cells usually precede growth inhibition. The chlorophyll content can therefore be used as a sensitive biomarker in plants exposed to exogenous chemicals (Iori et al., 2013). The results are shown in Fig. 3. The chlorophyll *a*, chlorophyll *b*, and total chlorophyll contents were markedly lower for the *L. minor* plants treated with Rac-, *R*-, and *S*-IM than for the control plants. The chlorophyll *a* contents of the cells were factors of 3.12, 1.76, and 3.67 lower in the plants treated with 0.5 mg/kg Rac-, *S*-, and *R*-IM, respectively, than in the control plants. The chlorophyll *b* contents of the cells were factors of 5.03, 2.96, and 3.43 lower in the plants treated with 0.5 mg/kg Rac-, *S*-, and *R*-IM, respectively, than in the control plants. The total chlorophyll contents of the cells were factors of 3.47, 1.98, and 3.6 lower in the plants treated with 0.5 mg/kg Rac-, *S*-, and *R*-IM, respectively, than in the control plants. The enantiomers of IM showed different effects on chlorophyll. Chlorophyll is involved in light collection, energy transfer, and light energy conversion, which are important for plant growth (Liu et al., 2018; Xiong et al., 2016). Therefore, it was inferred that IM inhibits *L. minor* growth by inhibiting chlorophyll. With the increase of toxicity, the inhibition of chlorophyll by IM was greater which can also indicate that the chlorophyll *a*, chlorophyll *b*, and total chlorophyll contents were negatively dependent on the IM concentration. The carotenoid contents were markedly lower in the plants exposed to 0.5 mg/L Rac- and *R*-IM than in the control plants. However, under other concentrations, the carotenoid content in *L. minor* had no significant change compared with the control group. The results indicated that the chlorophyll *a*, chlorophyll *b*, and total chlorophyll in *L. minor* were more sensitive than carotenoids, and could be used as biomarkers to assess the adverse effects of IM on photosynthesis by *L. minor*.

3.3. Effects on the protein content, MDA content, and antioxidant enzyme

In addition to direct toxicity to organisms, many pollutants can indirectly cause cellular stress by forming reactive oxygen species (ROS) and inducing oxidative stress (Kim et al., 2017). Lipid peroxidation is a process of ROS oxidation of biofilms after oxygen stress was enhanced. And the final product of lipid peroxidation is MDA, so MDA is often used as a biomarker of lipid peroxidation in plants exposed to pollutants (De Zwart et al., 1999). The MDA contents of the *L. minor* plants are shown in Fig. 4a. Markedly higher MDA contents were found for *L. minor* plants treated with three different IM concentrations than for the control plants. This indicated that lipids in the plants were oxidatively damaged because of exposure to IM and that antioxidant enzymes produced by the plants could not completely eliminate the reactive oxygen species (ROSs) that were produced (Huang et al., 2012). The highest MDA content was found for *L. minor* plants exposed to medium concentrations of Rac- and *R*-IM. This may be because *L. minor* possibly uses MDA at high concentrations to eliminate ROSs, meaning more MDA was used to remove ROSs at high IM concentrations than at medium IM concentrations (Liu et al., 2019). The results indicated that lipid peroxidation was induced to different degrees by the different IM enantiomers. Oxidative stress was found to be induced more strongly in *L. minor* by Rac- and *R*-IM than by *S*-IM.

Antioxidant enzymes (such as CAT, POD, and SOD) and antioxidants (such as glutathione) in plants play key roles in eliminating ROSs and decreasing oxidative damage. SOD is the first such enzyme in the antioxidant system that is produced when an organism reacts to oxidative stress. SOD can prevent superoxide anion radicals being produced by disproportionation of O^{2-} to give O_2 and H_2O_2 (Bi et al., 2012). The SOD activity results are shown in Fig. 4b. The SOD activities were higher in *L. minor* exposed to IM at the three test concentrations than in the control plants. This may have been caused by a self-protection mechanism in the plants aimed at preventing subsequent damage by IM. The SOD activity in *L. minor* increased markedly in a concentration-dependent manner as the Rac- and *R*-IM concentrations increased. The SOD activity of *R*-, Rac- and *S*-IM reached the maximum value at 0.5, 0.5 and 0.08 mg/kg, respectively, which was 1.33, 1.32 and 1.25 times of control plants. This indicated that the different IM enantiomers affected SOD activity in *L. minor* to different extents which were consistent with the results of Qian, he previously found that SOD activity in rice was affected to different extents by the enantiomers of imazethapyr (Qian et al., 2009).

Changes in CAT and POD activities are considered to be adaptations to stress in plants stimulated by various environmental and chemical stressors. CAT is the second line of defense against oxidative stress. When SOD fails to completely eliminate ROS, CAT and POD can reduce

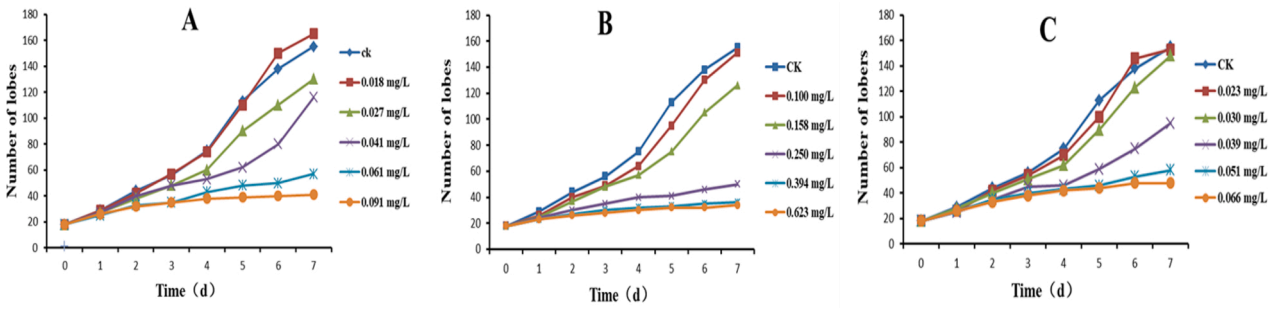

Fig. 2. Effects of (A) racemic imazamox, (B) *S*-imazamox, and (C) *R*-imazamox on the numbers of fronds on *Lemna minor* plants after 7 d exposure (CK = control).

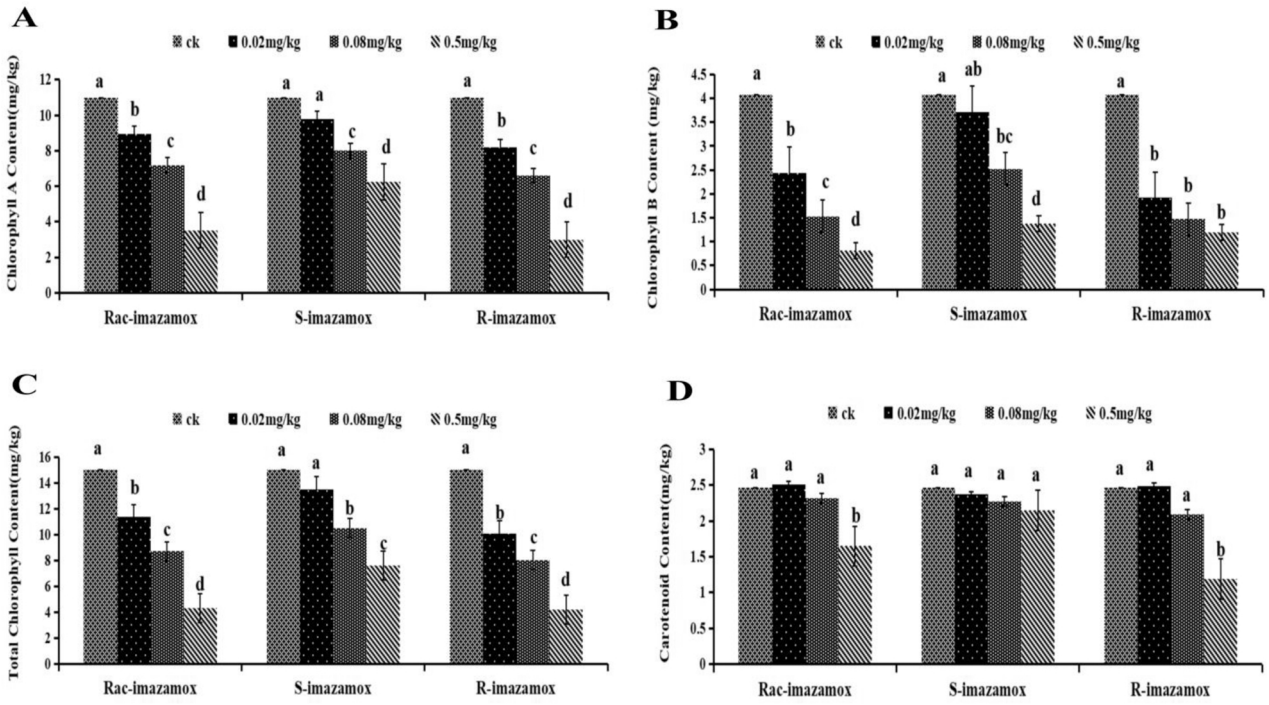

Fig. 3. Effects of racemic (Rac-), *S*-, and *R*-imazamox on the (A) chlorophyll *a*, (B) chlorophyll *b*, (C) total chlorophyll, and (D) carotenoid contents of *Lemna minor* after 7 d exposure. Different letters indicate significant differences ($P < 0.05$) between the mean photosynthetic pigment contents.

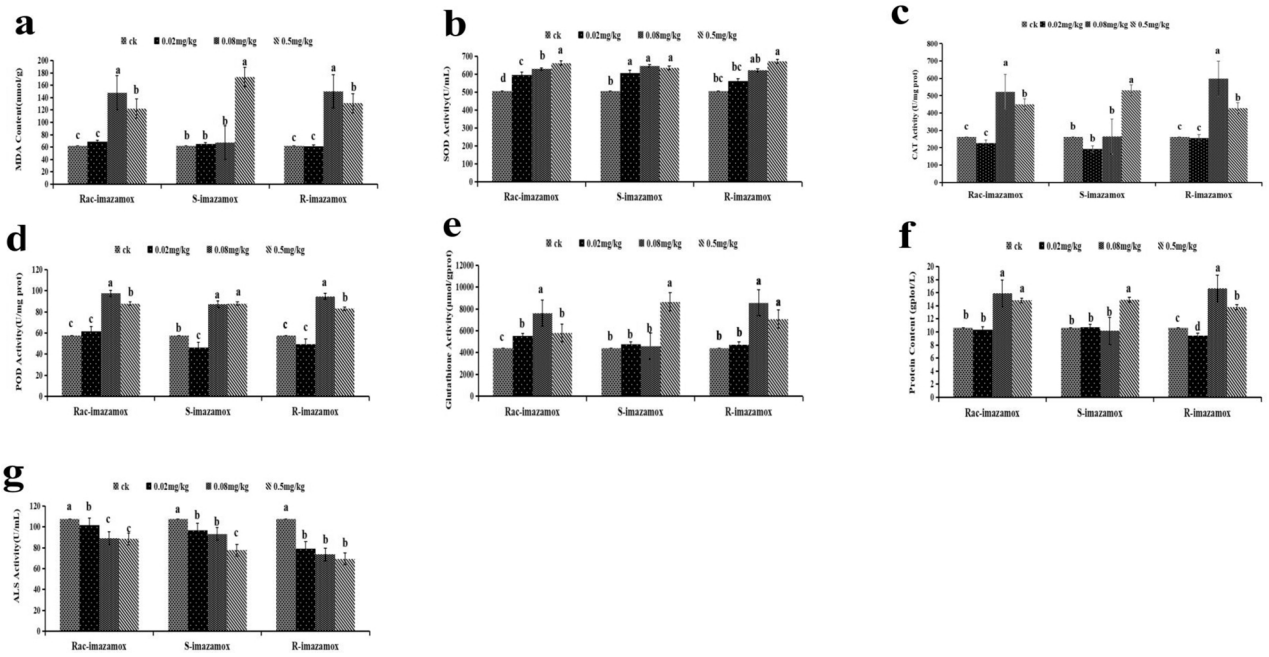

Fig. 4. Effects of racemic (Rac-), *S*-, and *R*-imazamox on the (a) malondialdehyde (MDA) and (f) protein contents and the (b) superoxide dismutase (SOD), (c) catalase (CAT), (d) peroxidase (POD), (e) glutathione (GSH), and (g) acetolactate synthase (ALS) activities of *Lemna minor* after 7 d exposure. Different letters indicate significant differences ($P < 0.05$) between the mean contents or activities.

H_2O_2 (Gomes et al., 2017; Zhao et al., 2012). The CAT and POD activities that were found were shown in Figs. 4c and 4d, respectively. The CAT and POD activities were higher for *L. minor* exposed to IM at different concentrations than for the control plants. The CAT and POD activities first increased and then decreased as the Rac- and *R*-IM concentrations increased. The activities of antioxidant enzymes in *L. minor* would have increased to prevent oxidative damage caused by IM (i.e., to achieve self-defense), but once the concentrations of ROSs exceeded the tolerable range, the excess ROSs produced would have inhibited antioxidant enzyme production (Tang et al., 2015). However, the CAT activities at *S*-IM concentrations of 0.02 and 0.08 mg/L and the control group were not significantly different which showed the enantiomers of IM had different effects on CAT activity. In a previous study it was found that antioxidant enzyme activity promotion and inhibition were controlled by the degree of stress exerted on the organism (Gao et al., 2020). The CAT and POD activities were affected to different degrees by

the different IM enantiomers. IM was found to cause oxidative damage in *L. minor*.

Glutathione can maintain cells in stable states and eliminate oxidative stress caused by ROSs. The glutathione activity was higher in *L. minor* treated with Rac-, *R*-, and *S*-IM than in the control plants, indicating that IM caused peroxidation of lipids in the plant cell membranes (Musgrave et al., 2013). As shown in Fig. 4e, the highest glutathione activities were found for *L. minor* exposed to 0.08 mg/L Rac- and *R*-IM. The glutathione activities in *L. minor* treated with 0.08 mg/L *R*- and Rac-IM were 1.95 and 1.73 times higher, respectively, than the glutathione activity in the control plants. The glutathione activity was markedly higher in the plants exposed to *S*-IM than in the control plants only at an *S*-IM concentration of 0.5 mg/L. This was consistent with the results of the acute toxicity tests, which indicated that *S*-IM was less toxic to *L. minor* at concentrations of 0.02 and 0.08 mg/L than at a concentration of 0.5 mg/L. These results indicated that the effects of IM on *L. minor* involve oxidative stress and that the different IM enantiomers affect the glutathione activity to different degrees.

As shown in Fig. 4f, the protein contents were higher in the plants exposed to IM than in the control plants. An increase in the protein content of a plant cell is believed to be a response to adverse conditions because the proteins produced can be degraded to provide free amino acids for the synthesis of enzymes for specific functions aimed at resisting adverse environmental conditions (Cooke et al., 1980). The antioxidant enzyme activities suggested that the protein content of *L. minor* may have increased because of the synthesis of functional proteins such as CAT, POD, and SOD.

By comprehensive analysis of the above results, it could be concluded that IM caused serious oxidative stress and lipid peroxidation damage in *L. minor*. And the enantiomers had significant different effects on *L. minor*.

3.4. Effects on the ALS activities

The ALS activity of Rac-IM and two enantiomers, showed in Fig. 4g, was calculated from the ALS calibration curve. And the correction curve of ALS was $Y= 0.0005X+ 0.0657$ ($R^2 =0.9919$). The ALS activities were markedly lower in *L. minor* exposed to Rac-, *R*-, and *S*-IM at different concentrations than in the control plants. The ALS activity gradually decreased as the IM concentration increased, meaning the ALS activity was negatively related to the IM toxicity. The ALS activities in *L. minor* treated with 0.5 mg/L *S*-,*R*- and Rac-IM were 1.38, 1.55 and 1.21 times lower than control, respectively. This suggested that the enantiomers of IM showed different effects on ALS. IM inhibited ALS synthesis and therefore may inhibit the synthesis of branched-chain amino acids and *L. minor* growth. The results suggested that the assumed mechanism through which IM affects *L. minor* was consistent with the known mechanism.

3.5. Metabolic responses to IM

The metabolite data acquired by performing wide-target metabolomics analyses indicated that IM markedly affected metabolism in *L. minor*. The variable importance plot values for orthogonal projections to latent structures discriminant analysis and the P values for T-tests (variable importance plot value ≥ 1 and T-test $p < 0.05$) were used to identify significantly different metabolites in the different treatment groups (Fig. S1). Compared with the control samples, there were 68, 43, and 71 different metabolites in the samples that had been exposed to 0.036 mg/kg Rac-, *S*-, and *R*-IM, respectively (Table S1). These metabolites were mainly alkaloids, amino acids and their derivatives, flavones, lipids, and nucleotides and their derivatives. Enrichment analysis indicated that Rac-IM and *R*-IM had similar effects on the metabolic pathways in *L. minor*. Both Rac-IM and *R*-IM strongly affected biosynthesis of secondary metabolites, carbon fixation during photosynthesis, carbon metabolism, glutathione metabolism, porphyrin and chlorophyll metabolism, and zeatin biosynthesis (Table S2). This may have been because Rac- and *R*-IM have similar toxicities. *S*-IM strongly affected isoquinoline alkaloid biosynthesis, the phenylalanine, tyrosine, and tryptophan biosynthesis pathways, phenylalanine metabolism, phenylpropane biosynthesis, and tyrosine metabolism (Table S2).

3.6. Transcriptional responses to IM

The RNA sequencing technique was used to identify DEGs in *L. minor* exposed to 0.036 mg/L Rac-, *R*-, and *S*-IM to investigate the mechanisms involved in the toxicity of IM to *L. minor* at the transcription level. DEGs are generally considered to have a false discovery rate of < 0.05 and $|\log_2 FC|$ values > 1. The volcano plots indicated the different effects of Rac-, *R*-, and *S*-IM on *L. minor* gene transcription. Compared with the control samples, there were 3107, 2580, and 134 DEGs in the *L. minor* samples that had been treated with *R*-, Rac-, and *S*-IM, respectively (Table S3). These results were consistent with the acute toxicity test results, indicating a relationship between the number of genes and the strength of the effect of the IM treatment. The biological significances of the DEGs were investigated by performing gene ontology and KEGG enrichment analyses. The DEGs in the samples treated with Rac- and *R*-IM were mainly related to carbon fixation during photosynthesis, glutathione metabolism, the pentose phosphate pathway, photosynthesis-antenna proteins, plant hormone signal transduction, and zeatin biosynthesis. The DEGs in the samples treated with *S*-IM were mainly related to phenylalanine metabolism, phenylpropanoid biosynthesis, plant hormone signal transduction, and zeatin biosynthesis (Table S4).

3.7. Integrating the omics results to identify the molecular mechanisms underlying enantioselective plant responses to IM

The metabolic pathways shared by different genes and different metabolites are shown in Fig. 5. Photosynthetic pigment is essential to photosynthesis because it absorbs the light that allows photosynthesis to occur. Exposing *L. minor* to *R*-IM affected porphyrin and chlorophyll metabolism. Glutamyl-tRNA reductase, magnesium chelatase subunit H, and chlorophyll *b* reductase are key enzymes involved in porphyrin and chlorophyll metabolism. Glutamyl-tRNA reductase catalyzes the transformation of glutamyl-tRNA into glutamate-1-semialdehyde and initiates biosynthesis of chlorophyll (Zeng et al., 2020). Magnesium chelatase subunit H catalyzes the insertion of Mg^{2+} into protoporphyrin IX to give Mg-protoporphyrin IX, which is the first step in the synthesis of chlorophyll (Zhang et al., 2018). *R*-IM caused the genes encoding glutamyl-tRNA reductase and magnesium chelatase subunit H to be downregulated, which could have inhibited chlorophyll synthesis. Chlorophyll *b* reductase catalyzes the degradation of chlorophyll *b* (Horie et al., 2009). Upregulation of the chlorophyll *b* reductase gene may have accelerated chlorophyll *b* degradation. This was consistent with the decrease in the photosynthetic pigment content found in the physiological and biochemical tests. The result showed that the expression of metabolites threonine and glutamate were increased. The expression of genes encoding enzymes that play key roles in chlorophyll synthesis were decreased (leading to accumulation of glutamate, which is essential to chlorophyll synthesis) and therefore decrease the chlorophyll content (Takano et al., 2020). Phosphorylation of threonine allows electron transfer to occur (Hansson et al., 2003). The increase in threonine expression found in this study indicated that less phosphorylation occurred and electron transfer was inhibited. This indicates that *R*-IM may inhibit photosynthetic pigment synthesis by affecting expression of genes and metabolites involved in chlorophyll synthesis and therefore decrease the amount of light absorbed by the plant.

Damage to chlorophyll may affect carbon fixation in a photosynthetic organism. Carbon fixation in a photosynthetic organism involves reactions facilitated by light to fix and reduce CO_2 to produce organic matter. In this study, Rac- and *R*-IM caused the genes related to key

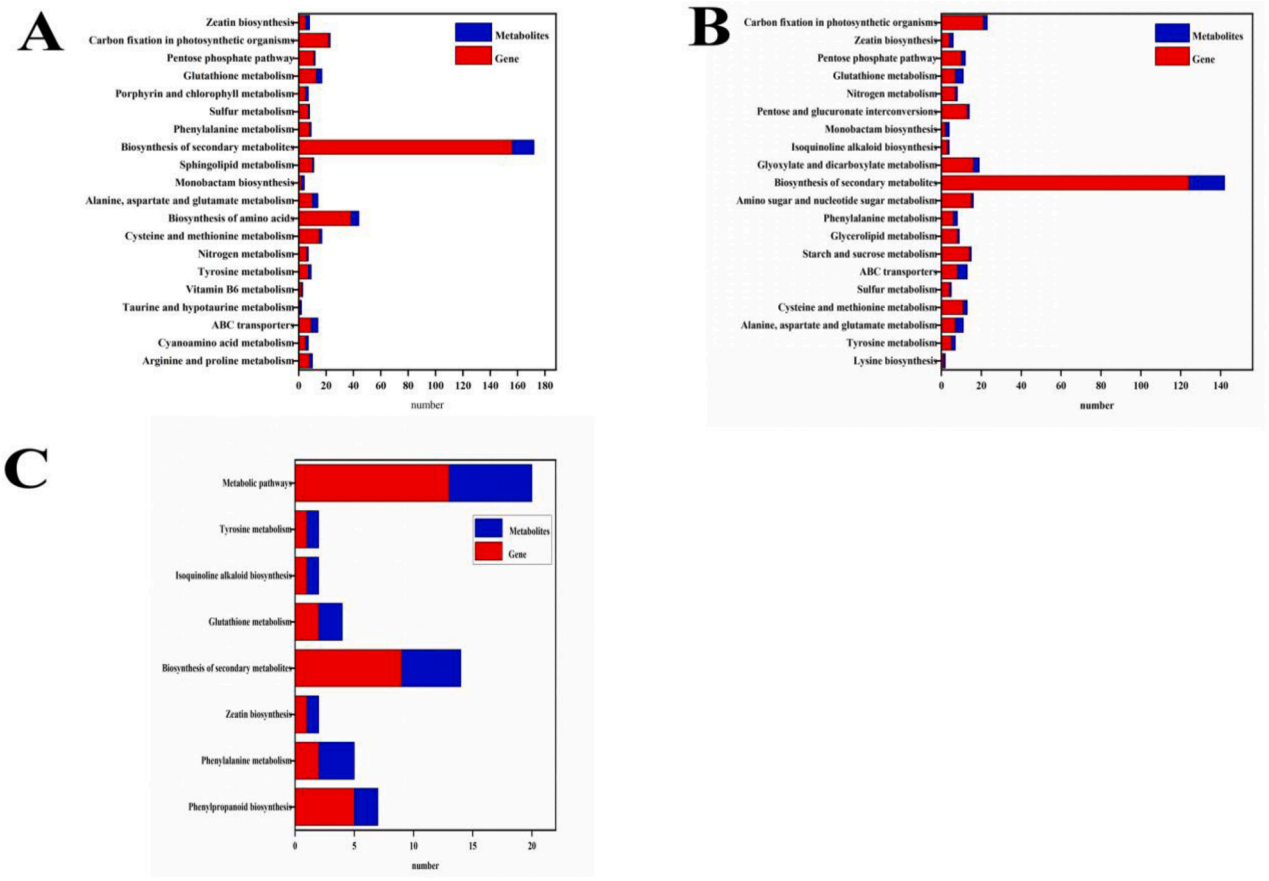

Fig. 5. Metabolic pathways shared by different metabolites and genes in *Lemna minor* treated with (A) *R*-imazamox, (B) racemic imazamox, and (C) *S*-imazamox.

enzymes that fix carbon (phosphoglycerate kinase, ribose 5-phosphate isomerase, and ribulose-bisphosphate carboxylase (small chain)) in *L. minor* to be downregulated. Ribulose-bisphosphate carboxylase (small chain) is a component of ribulose 1,5-bisphosphate carboxylase, which catalyzes the transformation of ribulose 1,5-bisphosphate into 3-phosphoglyceric acid. This is a key step that determines the photosynthetic carbon assimilation rate (Xiong et al., 2019). Phosphoglycerate kinase catalyzes the formation of 1,3-bisphosphoglycerate from 3-phosphoglycerate. Phosphoglycerate kinase is essential to gluconeogenesis (Li et al., 2019b). Ribose 5-phosphate isomerase catalyzes the formation of ribulose-5-phosphate from ribose-5-phosphate and therefore plays an important role in photosynthetic carbon fixation (Wang et al., 2013). However, decreased expression of the genes that encode these enzymes indicated that carbon fixation was inhibited. This would have affected the production of carbohydrates, which are the most important stores of energy that sustains all of the activities of plants. Rac- and *R*-IM may affect the growth, physiology, and biochemistry of *L. minor* by inhibiting carbohydrate production. Rac- and *R*-IM increased expression of glutamate and related genes that encode aspartic acid transferase. Glutamate is transformed into aspartic acid by aspartic acid transferase, so expression of the metabolite aspartic acid also increased. Aspartic acid is used widely in biosynthesis and is a precursor for the syntheses of various amino acids (De et al., 2014).

It has previously been found that carbon fixed in a photosynthetic organism is transformed through the gluconeogenic pathway and then the pentose phosphate metabolic pathway with glucose-6-phosphate as a precursor, which indicates that redox homeostasis can be affected by oxidative stress (Gruning et al., 2011). The oxidative part of the pentose phosphate pathway includes oxidation and decarboxylation of glucose 6-phosphate to give ribulose 5-phosphate, catalyzed by 6-phosphogluconate dehydrogenase enzymes, and then isomerization of ribulose 5-phosphate into ribose 5-phosphate, which is an important component of nucleotides (Karaman et al., 2020). However, in this study, genes related to ribulose 5-phosphate isomerase were downregulated by Rac- and *R*-IM, indicating that Rac- and *R*-IM may be toxic to *L. minor* by inhibiting nucleotide synthesis. Upregulation of the gene associated with 6-phosphate dehydrogenase indicated that more NADPH was produced. Upregulation of expression of the metabolite gluconic acid also provides energy for metabolism of pentose phosphate, which is also used in biosyntheses (Kumar et al., 2015). The pentose phosphate pathway is a multifunctional metabolic pathway. Rac- and *R*-IM may affect metabolism in *L. minor* by affecting genes and metabolites involved in the pentose phosphate pathway and may therefore affect the production of NADPH, intermediate metabolites, and products of the pentose phosphate pathway.

NADPH provided by the pentose phosphate pathway and the glutathione metabolic pathway co-regulates the glutathione redox system (Kizilbay et al., 2020). The results of this study indicated that Rac- and *R*-IM affect the glutathione metabolic pathway in *L. minor*. Glutathione is a simple tripeptide compound consisting of one glutamic acid unit, one cysteine unit, and one glycine unit. The active sulfhydryl group (–SH) in glutathione allows glutathione to participate in various in vivo biochemical reactions (Lu et al., 2013). The metabolite vitamin C and reduced glutathione contents were higher in plants treated with Rac- and *R*-IM than in the control plants. Vitamin C can maintain –SH in the reduced state and therefore maintain the activity of the enzyme and can transform oxidized glutathione into reduced glutathione and therefore reduce the H_2O_2 produced during metabolism. This is consistent with the glutathione activities found in this study. Rac- and *R*-IM treatment increased the glutathione activity in L. *minor* and therefore allowed excess ROSs to be eliminated.

Phenylalanine metabolism is central to plant metabolism and

promotes the transition from primary to secondary metabolism. Stable phenylalanine metabolism can ensure normal growth and development of the organism as well as normal physiology and biochemistry. In the phenylalanine metabolism pathway, phenylalanine is catalytically deaminated to cinnamic acid, which is a precursor for phenylpropane derivatives (Wang et al., 2016b). Phenylpropane is unique to plants and plays an important role in plant growth, development, and interactions with the environment. Phenylpropane can also act as a regulatory molecule and plays important roles in defenses against pathogens, signal transduction, and interactions with other organisms (Kim et al., 2015). Phenylalanine ammonialyase and caffeoyl-CoA O-methyltransferase (CCoAOMT) are key enzymes involved in phenylalanine metabolism and phenylpropanoid biosynthesis. Compared with the control plants, *S*-IM upregulated the genes that encode both phenylalanine ammonialyase and CCoAOMT. Phenylalanine ammonialyase is a key enzyme involved in the stress responses of plants, and expression and biosynthesis of phenylalanine ammonialyase can be upregulated by external stimuli (Li et al., 2012). CCoAOMT can respond to stressors and induce expression of the CCoAOMT gene to allow various adverse environmental (biological and abiotic) conditions to be resisted (Liu et al., 2015). CCoAOMT catalyzes the transformation of caffeoyl-CoA O-methyl into ferulic coenzyme A, which affects the synthesis of *S*-lignin and *G*-lignin (Ye et al., 2001; Lee et al., 1997). POD is a key enzyme involved in the phenylalanine metabolism pathway as well as the phenylpropanoid biosynthesis pathway that synthesizes lignin monomers. POD catalyzes the dehydrogenation polymerization reaction that allows lignin to form. Coniferin is a precursor of lignin. In this study, increased POD gene expression and coniferin expression may have increased the lignin contents of the plants. Lignin is a complex polymer of phenylpropane monomers and is an important component of cell walls, giving them rigidity that maintains the cell shape and provides mechanical support for the plant. Secondary lignification of cell walls plays a key role in plant growth and development and in resistance to biotic and abiotic stressors (Zhang et al., 2019). Cinnamic acid is converted into *p*-hydroxycinnamic acid by cinnamate-4-hydroxylase. The reaction catalyzed by cinnamate-4-hydroxylase marks the end of the early steps of the pentose phosphate pathway and represents the branching point of the pathway because *p*-hydroxycinnamic acid can be used to synthesize a series of metabolites such as lignin and flavonoids (Kurepa et al., 2018). The increase in the *p*-hydroxycinnamic acid content meant that more secondary metabolites were produced. The DEGs and metabolites mentioned above belonged to secondary metabolic pathways. The secondary metabolic pathways of plants provide many non-essential small-molecule compounds used by plant cells during normal plant growth. *S*-IM may have caused some secondary metabolites that could cope with the toxicity of *S*-IM to *L. minor* to be formed by affecting expression of key genes and metabolites in the phenylalanine metabolism and phenylpropanoid biosynthesis pathways.

Importantly, zeatin biosynthesis in *L. minor* was affected by Rac-, *R*-, and *S*-IM. Cytokinins control cell division by interacting with other plant hormones, participate in various plant growth and development processes, regulate chloroplast differentiation during the maturation process, and respond to various biological and abiotic stresses (Cortleven et al., 2019). The main cytokinins are *trans*-zeaxin and isoprene adenine cytokinins (Miyawaki et al., 2006). Cytokinin dehydrogenase, cytokinin *trans*-hydroxylase, and isopentenyl transferase are the three key enzymes involved in zeatin synthesis. Isoprene transferases catalyze AMP/ADP/ATP and dimethylallyl diphosphate reactions and therefore catalyze cytokinin biosynthesis (Kakimoto, 2001; Takei et al., 2001). Two cytoplasmic P450 enzymes, CYP735A1 and CYP735A2, can cause *trans*-zeaxin nucleotides to form (Takei et al., 2004). In this study, the isoprene transferase gene IPT5 and CYP735A2 contents were higher in the plants treated with Rac- and *R*-IM than the control plants, indicating that gene upregulation may have accelerated *trans*-zeaxin production. Cytokinin dehydrogenase is the key enzymes involved in zeatin synthesis and the only enzyme that is known to catalyze the irreversible inactivation of cytokinin (Opio et al., 2020). Rac-, *R*-, and *S*-IM reduced the expression of CKX10 gene associated with cytokinin. In the zeatin biosynthesis pathway, IM promoted the synthesis of cytokinin in *L. minor*, inhibited the decomposition of cytokinin, and then led to the accumulation of cytokinin in vivo. The accumulation of cytokinin inhibits the growth of lateral and coronal roots and the absorption of zinc by crops, thus affecting the growth, development and yield of the whole plant (Laplaze et al., 2007).

And more importantly, Rac- and *R*-IM had similar effects on multiple metabolic pathways in *L. minor* which were mainly related to photosynthesis and antioxidant. It may explain that Rac- and *R*-IM had similar toxicities to *L. minor*. However, *S*-IM mainly affected *L. minor* by multiple metabolic pathways associated with secondary metabolites. Therefore, it can be inferred that the enantioselective toxicity of enantiomers of IM to *L. minor* may be caused by its effects on different genes and metabolites involved in different metabolic pathways.

3.8. qRT-PCR validation

The transcriptome results were validated by the analysis of random selection of seven DEGs by qRT-PCR. The expression results for the seven DEGs were consistent with the transcriptomic data (Fig. 6), indicating that the transcriptomic analysis results were reliable.

4. Conclusions

This study comprehensively and systematically evaluated the enantioselective toxicity mechanism of imazamox to *L. minor* from enantiomer level. EC_{50} values showed that the toxicity of Rac- and *R*-IM to *L. minor* was significantly higher than that of *S*-IM, showing enantioselectivity. In addition, imazamox and its enantiomers had significantly different effects on physiological and biochemical systems of *L. minor*. IM decreased the photosynthetic pigment content and ALS activity but increased the MDA and protein contents, as well as the activities of CAT, glutathione, POD, and SOD. What's more the different effects were closely related to pollution levels. Further, the metabonomics and transcriptome correlation analysis was used for the first time to reveal the toxicity mechanism of imazamox to *L. minor*. The results showed that the differential genes and metabolites in *L. minor* exposed to *R*-IM were significantly more than those in *S*-IM which was consistent with enantioselective toxicity. Under *S*-IM exposure, differential genes and metabolites were mainly enriched in multiple metabolic pathways associated with secondary metabolites including phenylalanine metabolism, phenylpropanoid biosynthesis, and secondary metabolite biosynthesis. *R*-IM and Rac-IM affected *L. minor* by multiple metabolic pathways related to photosynthesis and antioxidant including carbon fixation during photosynthesis, the glutathione metabolic pathway and the pentose phosphate pathway. *R*-IM also disturbance porphyrin and chlorophyll metabolism. Zeatin biosynthesis was markedly affected by Rac-, *R*-, and *S*-IM. These results indicated that IM had enantioselective toxicity to *L. minor* and could cause oxidative stress and damage to *L. minor*. Enantioselective IM toxicity to *L. minor* may be caused by the different enantiomers affecting genes and metabolites involved in different metabolic pathways. Previously unknown mechanisms were found to be involved in the toxicity of IM to *L. minor*, and this information will be useful in terms of improving guidance for the use of IM and better assessing its safety.

CRediT authorship contribution statement

Rui Li: Methodology, Writing – original draft, Writing – review & editing, Investigation, Data curation. **Chenxi Luo:** Data curation, Investigation. **Jingsi Qiu:** Validation, Investigation. **Yuanfu Li:** Validation, Investigation. **Hui Zhang:** Writing – review & editing, Data curation. **Huihua Tan:** Resources, Writing – review & editing, Supervision, Data curation, Project administration.

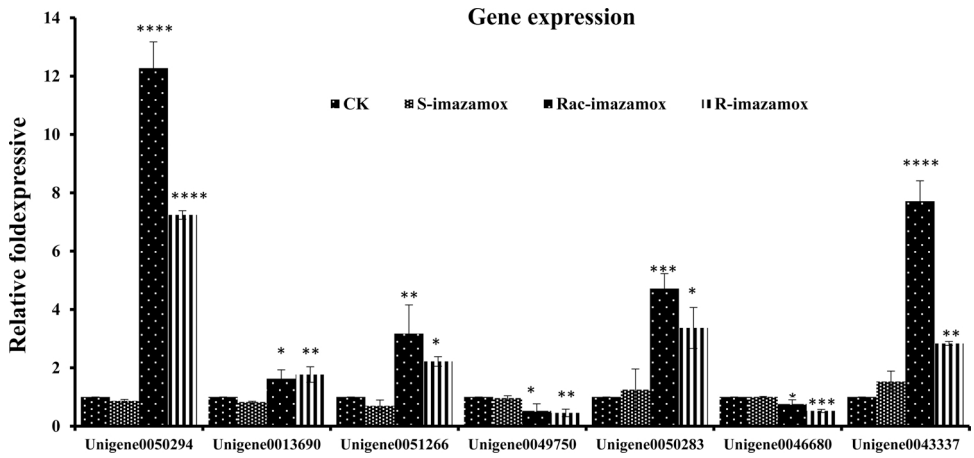

Fig. 6. Expression levels of genes in control *Lemna minor* plants (CK) and *Lemna minor* plants exposed to *S*-, racemic (Rac-), and *R*-imazamox.

Declaration of Competing Interest

The authors declare that they have no known competing financial interests or personal relationships that could have appeared to influence the work reported in this paper.

Acknowledgements

This work was supported by National Natural Science Foundation of China (grant no. 31872000).

Appendix A. Supporting information

Supplementary data associated with this article can be found in the online version at doi:10.1016/j.jhazmat.2021.127818.

References

Asada, M.A.U., Lavoie, M., Song, H., Jin, Y.J., Fu, Z.W., Qian, H.F., 2017. Interaction of chiral herbicides with soil microorganisms, algae and vascular plants. Sci. Total. Environ. 580, 1287–1299. https://doi.org/10.1016/j.scitotenv.2016.12.092.

Bi, Y.F., Miao, S.S., Lu, Y.C., Chong, B.Q., Zhou, Y., Yang, H., 2012. Phytotoxicity, bioaccumulation and degradation of isoproturon in green algae. J. Hazard. Mater. 243, 242–249. https://doi.org/10.1016/j.jhazmat.2012.10.021.

Cessna, A.J., Elliott, J.A., Bailey, J., 2012. Leaching of three imidazolinone herbicides during sprinkler irrigation. J. Environ. Qual. 41, 882–892. https://doi.org/10.2134/jeq2011.0198.

Chiaia-Hernandez, A.C., Keller, A., Wachter, D., Steinlin, C., Camenzuli, L., Hollender, J., Krauss, M., 2017. Long-term persistence of pesticides and TPs in archived agricultural soil samples and comparison with pesticide application. Environ. Sci. Technol. 51, 10642–10651. https://doi.org/10.1021/acs.est.7b02529.

Chen, Z.W., Song, S.F., Wen, Y.Z., Zou, Y.Q., Liu, H.J., 2016. Toxicity of cu (ii) to the green alga *Chlorella vulgaris*: a perspective of photosynthesis and oxidant stress. Environ. Sci. Pollut. Res. 23, 17910–17918. https://doi.org/10.1007/s11356-016-6997-2.

Cooke, R.J., Roberts, K., Davies, D.D., 1980. Model for stress-induced protein degradation in *Lemna minor*. Plant Physiol. 66, 1119–1122. https://doi.org/10.1104/pp.66.6.1119.

Cortleven, A., Leuendorf, J.E., Frank, M., Pezzetta, D., Bolt, S., Schmülling, T., 2019. Cytokinin action in response to abiotic and biotic stress in plants. Plant Cell Environ. 42, 998–1018. https://doi.org/10.1111/pce.13494.

De, L.T.F., El-Azaz, J., Avila, C., Canovas, F.M., 2014. Deciphering the role of aspartate and prephenate aminotransferase activities in plastid nitrogen metabolism. Plant Physiol. 164, 92–104. https://doi.org/10.1104/pp.113.232462.

De Zwart, L.L., Meerman, J.H.N., Commandeur, J.N.M., Vermeulen, N.P.E., 1999. Biomarkers of free radical damage applications in experimental animals and in humans. Free Radic. Biol. Med. 26, 202–226. https://doi.org/10.1016/S0891-5849(98)00196-8.

FAOSTAT, 2017. FAO Statistical Databases. (https://www.fao.org/faostat/en/#search/Pesticides%20total).

Gao, J., Wang, F., Jiang, W.Q., Miao, J.W., Wang, P., Zhou, Z.Q., Liu, D.H., 2020. A full evaluation of chiral phenylpyrazole pesticide flufiprole and the metabolites to non-target organism in paddy field. Environ. Pollut. 264. https://doi.org/10.1016/j.envpol.2020.114808.

Gomes, M.P., Goncalves, C.A., Cesar, J., de Brito, J.C.M., Souza, A.M., Cruza, F.V.D.S., Bicalho, E.M., Figueredo, C.C., Garci, Q.S., 2017. Ciprofloxacin induces oxidative stress in duckweed (*Lemna minor L.*): implications for energy metabolism and antibiotic-uptake ability. J. Hazard. Mater. 328, 140–149. https://doi.org/10.1016/j.jhazmat.2017.01.005.

Gruning, N.M., Rinnerthaler, M., Bluemlein, K., Mulleder, M., Wamelink, M.M.C., Lehrach, H., Jakobs, C., Breitenbach, M., Ralser, M., 2011. Pyruvate kinase triggers a metabolic feedback loop that controls redox metabolism in respiring cells. Cell Metab. 3, 415–427. https://doi.org/10.1016/j.cmet.2011.06.017.

Hansson, M., Vener, A.V., 2003. Identification of three previously unknown in vivo protein phosphorylation sites in thylakoid membranes of *Arabidopsis thaliana*. Mol. Cell. Proteom. 2, 550–559. https://doi.org/10.1074/mcp.M300050-MCP200.

Horie, Y., Ito, H., Kusaba, M., Tanaka, R., Tanakaet, A., 2009. Participation of chlorophyll *b* reductase in the initial step of the degradation of light-harvesting chlorophyll *a/b*-protein complexes in *Arabidopsis*. J. Biol. Chem. 284, 17449–17456. https://doi.org/10.1074/jbc.M109.008912.

Hu, M.F., Liu, K.F., Qiu, J.S., Zhang, H., Li, X.S., Zeng, D.Q., Tan, H.H., 2020. Behavior of imidazolinone herbicide enantiomers in earthworm-soil microcosms: degradation and bioaccumulation. Sci. Total Environ. 707, 135476–135484. https://doi.org/10.1016/j.scitotenv.2019.135476.

Huang, L.D., Lu, D.H., Diao, J.L., Zhou, Z.Q., 2012. Enantioselective toxic effects and biodegradation of benalaxyl in *Scenedesmus obliquus*. Chemosphere 87, 7–11. https://doi.org/10.1016/j.chemosphere.2011.11.029.

Iori, V., Zacchini, M., Pietrini, F., 2013. Growth, physiological response and phytoremoval capability of two willow clones exposed to ibuprofen under hydroponic culture. J. Hazard. Mater. 262, 796–804. https://doi.org/10.1016/j.jhazmat.2013.09.017.

Kakimoto, T., 2001. Identification of plant cytokinin biosynthetic enzymes as dimethylallyl diphosphate:atp/adp isopentenyl transferases. Plant Cell Physiol. 42, 677–685. https://doi.org/10.1093/pcp/pce112.

Kanehisa, M., Araki, M., Goto, S., Hattori, M., Hirakawa, M., Itoh, M., Katayama, T., Kawashima, S., Okuda, S., Tokimatsu, T., Yamanishi, Y., 2008. KEGG for linking genomes to life and the environment. Nucleic Acids Res. 36, 480–484. https://doi.org/10.1093/nar/gkm882.

Karaman, M., Temel, Y., Bayindir, S., 2020. Inhibition effect of rhodanines containing benzene moieties on pentose phosphate pathway enzymes and molecular docking. J. Mol. Struct. 1220, 128700 https://doi.org/10.1016/j.molstruc.2020.128700.

Kim, H.R., Shin, D.Y., Chung, K.H., 2017. In vitro inflammatory effects of polyhexamethylene biguanide through NF-kappa B activation in A549 cells. Toxicol. Vitr. 38, 1–7. https://doi.org/10.1016/j.tiv.2016.10.006.

Kim, S., Kim, H., Park, A., Park, J.H., Lee, Y., Kim, Y.J., Han, T., Choi, E.Mi, 2015. The antioxidant response of *Lemna paucicostata* upon phenol exposure. Toxicol. Environ. Health Sci. 7, 73–81. https://doi.org/10.1007/s13530-015-0223-3.

Kizilbay, G., Karaman, M., 2020. Possible inhibition mechanism of dobutamine hydrochloride as potent inhibitor for human glucose-6-phosphate dehydrogenase enzyme. J. Biomol. Struct. Dyn. 1, 1–9. https://doi.org/10.1080/07391102.2020.1811155.

Klementová, S., Hornychova, L., Sorf, M., Zemanova, J., Kahoun, D., 2019. Toxicity of atrazine and the products of its homogeneous photocatalytic degradation on the aquatic organisms *Lemna minor* and *Daphnia magna*. Environ. Sci. Pollut. Res. 26, 27259–27267. https://doi.org/10.1007/s11356-019-05710-0.

Kumar, A., Rai, L.C., 2015. Proteomic and biochemical basis for enhanced growth yield of *Enterobacter sp*. LCR1 on insoluble phosphate medium. Microbiol. Res. 170, 195–204. https://doi.org/10.1016/j.micres.2014.06.006.

Kurepa, J., Shull, T.E., Karunadasa, S.S., Smalle, J.A., 2018. Modulation of auxin and cytokinin responses by early steps of the phenylpropanoid pathway. BMC Plant Biol. 18, 278. https://doi.org/10.1186/s12870-018-1477-0.

Laplaze, L., Benkova, E., Casimiro, I., Maes, L., Vanneste, S., Swarup, R., Weijers, D., Calvo, V., Parizot, B., Herrera-Rodriguez, M.B., Offringa, R., Graham, N., Doumas, P., Friml, J., Bogusz, D., Beeckman, T., Bennett, M., 2007. Cytokinins act directly on lateral root founder cells to inhibit root initiation, 3889-39 Plant Cell. 19. https://doi.org/10.1105/tpc.107.055863.

Lee, D., Meyer, K., Chapple, C., Douglas, C.J., 1997. Antisense suppression of 4-coumarate:coenzyme A ligase activity in *Arabidopsis* leads to altered lignin subunit composition. Plant Cell. 9, 1985–1998. https://doi.org/10.1105/tpc.9.11.1985.

Lee, H., Sung, E.J., Seo, S., Min, E.K., Lee, J.Y., Shim, I., Kim, P., Kim, T.Y., Lee, S., Kim, K.T., 2021. Integrated multi-omics analysis reveals the underlying molecular mechanism for developmental neurotoxicity of perfluorooctanesulfonic acid in zebrafish. Environ. Int. 157. https://doi.org/10.1016/j.envint.2021.106802.

Lewis, M.A., 1995. Use of freshwater plants for phytotoxicity testing: a review. Environ. Pollut. 87, 319–336. https://doi.org/10.1016/0269-7491(94)P4164-J.

Li, B., Dewey, C.N., 2011. RSEM: accurate transcript quantification from RNA-Seq data with or without a reference genome. BMC Bioinform. 12, 323. https://doi.org/10.1186/1471-2105-12-323.

Li, C.L., Bai, Y.C., Chen, H., Zhao, H.X., Shao, J.R., Wu, Q., 2012. Cloning, characterization and functional analysis of a phenylalanine ammonia-lyase gene (FtPAL) from *Fagopyrum tataricum Gaertn*. Plant Mol. Biol. Rep. 30, 1172–1182. https://doi.org/10.1007/s11105-012-0431-9.

Li, R., Hu, M.F., Liu, K.F., Zhang, H., Li, X.S., Tan, H.H., 2019a. Trace enantioselective determination of imidazolinone herbicides in various food matrices using a modified QuEChERS method and Ultra-Performance Liquid Chromatography/Tandem Mass Spectrometry. Food Anal. Meth. 12, 2647–2664. https://doi.org/10.1007/s12161-019-01607-3.

Li, R.Z., Qiu, Z.M., Wang, X., Gong, X.G., Xu, P.P., Yu, Q.Z., Guan, Y.F, Q.B., 2019b. Pooled CRISPR/Cas9 reveals redundant roles of plastidial phosphoglycerate kinases in carbon fixation and metabolism. Plant J. 6, 1078–1089. https://doi.org/10.1111/tpj.14303.

Li, Y.F., Zhang, Q.N., Yu, Y.F., Li, X.S., Tan, H.H., 2020. Integrated proteomics, metabolomics and physiological analyses for dissecting the toxic effects of halosulfuron-methyl on soybean seedlings (*Glycine max merr.*). Plant Physiol. Biochem. 157, 303–315. https://doi.org/10.1016/J.PLAPHY.2020.10.033.

Liu, W., Li, J.W., Gao, L.C., Zhang, Z., Zhao, J., He, X., Zhang, X., 2018. Bioaccumulation and effects of novel chlorinated polyfluorinated ether sulfonate in freshwater *alga scenedesmus obliquus*. Environ. Pollut. 233, 8–15. https://doi.org/10.1016/j.envpol.2017.10.039.

Liu, C.X., Liu, S.Z., Diao, J.L., 2019. Enantioselective growth inhibition of the green algae (*Chlorella vulgaris*) induced by two paclobutrazol enantiomers. Environ. Pollut. 250, 610–617. https://doi.org/10.1016/j.envpol.2019.04.027.

Lichtenthaler, H.K., 1987. Chlorophylls and carotenoids: Pigments of photosynthetic biomembranes. Methods Enzymol 148, 350–382. https://doi.org/10.1016/0076-6879(87)48036-1.

Liu, Y.X., Zou, D.M., Wu, B.S., Lin, D.H., Zhang, Z.H., Wu, J.C., 2015. Cloning and expression analysis of a CCoAOMT homolog in loquat fruit in response to low-temperature storage. Postharvest Biol. Tec. 105, 45–50. https://doi.org/10.1016/j.postharvbio.2015.03.008.

Lu, S.C., 2013. Glutathione synthesis. BBA-BIOMEMBRANES 1830, 3143–3153. https://doi.org/10.1016/j.bbagen.2012.09.008.

Mao, X.Z., Cai, T., Olyarchuk, J.G., Wei, L.P., 2005. Automated genome annotation and pathway identification using the KEGG Orthology (KO) as a controlled vocabulary. Bioinformatics 21, 3787–3793. https://doi.org/10.1093/bioinformatics/bti430.

Miyawaki, K., Tarkowski, P., Matsumoto, K.M., Kato, T., Sato, S., Tarkowska, D., Tabata, S., Sandberg, G., Kakimoto, T., 2006. Roles of arabidopsis atp/adp isopentenyltransferases and trna isopentenyltransferases in cytokinin biosynthesis. Proc. Natl. Acad. Sci. U. S. A. 103, 16598–16603. https://doi.org/10.1073/pnas.0603522103.

Musgrave, W.B., Yi, H., Kline, D., Cameron, J.C., Wignes, J., Dey, S., Pakrasi, H.B., Jez, J. M., 2013. Probing the origins of glutathione biosynthesis through biochemical analysis of glutamate-cysteine ligase and glutathione synthetase from a model photosynthetic prokaryote. Biochem. J. 450, 63–72. https://doi.org/10.1042/BJ20121332.

Opio, P., Tomiyama, H., Saito, T., Ohkawa, K., Ohara, H., Kondo, S., 2020. Paclobutrazol elevates auxin and abscisic acid, reduces gibberellins and zeatin and modulates their transporter genes in marubakaido apple (*Malus prunifolia borkh.* var. *ringo asami*) rootstocks. Plant Physiol. Biochem. 155, 502–511. https://doi.org/10.1016/j.plaphy.2020.08.003.

Park, J.S., Brown, M.T., Han, T., 2012. Phenol toxicity to the aquatic macrophyte *Lemna paucicostata*. Aquat. Toxicol. 106, 182–188. https://doi.org/10.1016/j.aquatox.2011.10.004.

Purkait, D., Hameed, S., Fatima, Z., 2021. Pathogen-omics: challenges and prospects in research and clinical settings. Arch. Toxicol. 94, 371–388. https://doi.org/10.1007/978-981-16-0691-5_28.

Qian, H.F., Han, X., Zhang, Q.N., Sun, Z.Q., Sun, L.W., Fu, Z.W., 2013. Imazethapyr enantioselectively affects chlorophyll synthesis and photosynthesis in *Arabidopsis thaliana*. J. Agric. Food Chem. 61, 1172–1178. https://doi.org/10.1021/jf305198g.

Qian, H.F., Hu, H.J., Mao, Y.Y., Ma, J., Zhang, A.P., Liu, W.P., Fu, Z.W., 2009. Enantioselective phytotoxicity of the herbicide imazethapyr in rice. Chemosphere 76, 885–892. https://doi.org/10.1016/j.chemosphere.2009.05.009.

Qian, H.F., Wang, R.Q., Hu, H.J., Lu, T., Chen, X.L., Ye, H.Q., Liu, W.P., Fu, Z.W., 2011. Enantioselective phytotoxicity of the herbicide imazethapyr and its effect on rice physiology and gene transcription. Environ. Sci. Technol. 45, 7036–7043. https://doi.org/10.1021/es200703v.

Sikorski, L., Baciak, M., Bes, A., Adomas, B., 2019. The effects of glyphosate-based herbicide formulations on *Lemna minor*, a non-target species. Aquat. Toxicol. 209, 70–80. https://doi.org/10.1016/j.aquatox.2019.01.021.

Takano, H.K., Beffa, R., Preston, C., Westra, P., Dayan, F.E., 2020. Glufosinate enhances the activity of protoporphyrinogen oxidase inhibitors. Weed Sci. 4, 324–332. https://doi.org/10.1017/wsc.2020.39.

Takei, K., Sakakibara, H., Sugiyama, T., 2001. Identification of genes encoding adenylate isopentenyltransferase, a cytokinin biosynthesis enzyme, in *Arabidopsis thaliana*. J. Biol. Chem. 276, 26405–26410. https://doi.org/10.1074/jbc.M102130200.

Tang, J., Zhang, Y., Cui, Y., Ma, J., 2015. Effects of a rhizobacterium on the growth of and chromium remediation by *Lemna minor*. Environ. Sci. Pollut. Res. 22, 9686–9693. https://doi.org/10.1007/s11356-015-4138-y.

Takei, K., Yamaya, T., Sakakibara, H., 2004. Arabidopsis CYP735A1 and CYP735A2 Encode Cytokinin Hydroxylases That Catalyze the Biosynthesis of trans-Zeatin. J. Biol. Chem. 279, 41866–41872. https://doi.org/10.1074/jbc.M406337200.

Tang, X.F., You, L., Liu, D., Xia, M., He, L.Y., Liu, H., 2019. 5-Hydroxyhexanoic acid predicts early renal functional decline in type 2 diabetes patients with microalbuminuria. Kidney Blood Press R. 44, 245–263. https://doi.org/10.1159/000498962.

Tian, S.N., Yan, S., Meng, Z.Y., Huang, S.R., Sun, W., Jia, M., Teng, M.M., Zhou, Z.Q., Zhu, W.T., 2021. New insights into bisphenols induced obesity in zebrafish (*Danio rerio*): activation of cannabinoid receptor CB1. J. Hazard. Mater. 418 https://doi.org/10.1016/j.jhazmat.2021.126100.

Wang, F., Liu, D.H., Qu, H., Chen, L., Zhou, Z.Q., Wang, P., 2016a. A full evaluation for the enantiomeric impacts of lactofen and its metabolites on aquatic macrophyte *Lemna minor*. Water Res. 101, 55–63. https://doi.org/10.1016/j.watres.2016.05.064.

Wang, J., Yang, W.T., 2013. Concerted proton transfer mechanism of *Clostridium thermocellum* ribose-5-phosphate isomerase. J. Phys. Chem. B 117, 9354–9361. https://doi.org/10.1021/jp404948c.

Wang, X., Wang, L.J., Yan, X.C., Wang, L., Tan, M.L., Geng, X.X., Wei, W.H., 2016b. Transcriptome analysis of the germinated seeds identifies low-temperature responsive genes involved in germination process in *Ricinus communis*. Acta Physiol. Plant. 38, 6. https://doi.org/10.1007/s11738-015-1994-5.

Wang, Y., Zhang, X.F., Yang, S.L., Yuan, Y.B., 2018. Lignin involvement in programmed changes in peach-fruit texture Indicated by metabolite and transcriptome analyses. J. Agric. Food Chem. 66, 12627–12640. https://doi.org/10.1021/acs.jafc.8b04284.

Wei, J., Zhang, X.X., Li, X.S., Zeng, D.Q., Tan, H.H., 2016. Enantioselective phytotoxicity of imazamox against maize seedlings. Bull. Environ. Contam. Toxicol. 96, 242–247. https://doi.org/10.1007/s00128-015-1682-6.

Xiong, J.Q., Kurade, M.B., Abou-Shanab, R.A.I., Ji, M.K., Choi, J., Kim, J.O., Jeon, B.H., 2016. Biodegradation of carbamazepine using freshwater microalgae *Chlamydomonas mexicana* and *Scenedesmus obliquus* and the determination of its metabolic fate. Bioresour. Technol. 205, 183–190. https://doi.org/10.1016/j.biortech.2016.01.038.

Xiong, Q.Q., Zhong, L., Shen, T.H., Cao, C.H., He, H.H., Chen, X.R., 2019. iTRAQ-based quantitative proteomic and physiological analysis of the response to N deficiency and the compensation effect in rice. BMC Genom. 20, 681. https://doi.org/10.1186/s12864-019-6031-4.

Yang, Y., Liu, P., Li, M., 2020. Tri-n-butyl phosphate induced earthworm intestinal damage by influencing nutrient absorption and energy homeostasis of intestinal epithelial cells. J. Hazard. Mater. 398. https://doi.org/10.1016/j.jhazmat.2020.122850.

Ye, J., Zhao, M.R., Niu, L.L., Liu, W.P., 2015. Enantioselective environmental toxicology of chiral pesticides. Chem. Res. Toxicol. 28, 325–338. https://doi.org/10.1021/tx500481n.

Ye, Z.H., Zhong, R.Q., Morrison, W.H., Himmelsbach, D.S., 2001. Caffeoyl coenzyme a O-methyltransferase and lignin biosynthesis. Phytochemistry 57, 1177–1185. https://doi.org/10.1016/S0031-9422(01)00051-6.

Young, M.D., Wakefield, M.J., Smyth, G.K., Oshlack, A., 2010. Gene ontology analysis for RNA-seq: accounting for selection bias. Genome Biol. 11, R14. https://doi.org/10.1186/gb-2010-11-2-r14.

Zeng, Z.Q., Lin, T.Z., Zhao, J.Y., Zheng, T.H., Xu, L.F., Wang, Y.H., Liu, L.L., Jiang, L., Chen, S.H., Wan, J.M., 2020. OsHemA gene,encoding glutamyl-tRNA reductase (GluTR) is essential for chlorophyll biosynthesis in rice(*Oryza sativa*). J. Integr. Agric. 19, 612–623. https://doi.org/10.1016/S2095-3119(19)62710-3.

Zhang, D., Chang, E.J., Yu, X.X., Chen, Y.H., Yang, Q.S., Cao, Y.T., Li, X.K., Wang, Y.H., Fu, A.G., Xu, M., 2018. Molecular characterization of magnesium chelatase in soybean [*Glycine max (L.) Merr.*]. Front. Plant Sci. 9, 720. https://doi.org/10.3389/fpls.2018.00720.

Zhang, W.J., Cheng, C., Chen, L., Di, S.S., Liu, C.X., Diao, J.L., Zhou, Z.Q., 2016. Enantioselective toxic effects of cyproconazole enantiomers against Chlorella pyrenoidosa. Chemosphere 159, 50–57. https://doi.org/10.1016/j.chemosphere.2016.05.073.

Zhang, Y., Hu, X.Q., Zheng, Y.Q., Liu, X.M., 2019. Ectopic expression of an antisense BpCCoAOMT gene from Betula platyphylla Suk. affects growth and development of tobacco due to lignin content reduction. J. Plant Biochem. Biot. 29, 266–275. https://doi.org/10.1007/s13562-019-00533-z.

Zhao, L., Peng, B., Hernandez-Viezcas, J.A., Rico, C., Sun, Y., Peralta-Videa, J.R., Tang, X. L., Niu, G.H., Jin, L.X., Varela, R.A., Zhang, J.Y., Gardea, T.J.L., 2012. Stress response and tolerance of Zea mays to CeO_2 nanoparticles: cross talk among H_2O_2, heat shock protein, and lipid peroxidation. ACS Nano 6, 9615–9622. https://doi.org/10.1021/nn302975u.

Zhou, J.A., Wu, Z.H., Yu, D., Yang, L., 2020. Toxicity of the herbicide flurochloridone to the aquatic plants *Ceratophyllum demersum* and *Lemna minor*. Environ. Sci. Pollut. Res. 27, 3923–3932. https://doi.org/10.1007/s11356-019-06477-0.